Spatio-Temporal Self-Focusing in Femtosecond Pulse Transmission Through Multimode Optical Fibers

Graham D. Hesketh, Francesco Poletti, *Member IEEE,* and Peter Horak

***Abstract*—We numerically investigate ultra-short pulse propagation in multimode optical fibers with launch peak powers approaching the critical power for self-focusing using a generalized multimode nonlinear Schrödinger equation approach. Nonlinear spatial and temporal effects combined with fiber dispersion govern pulse compression in space and time which can result in damage-inducing intensity levels. Here we identify pulse parameters for which damage is avoided and high-power delivery through optical fiber is possible near the fiber zero-dispersion wavelength.**

***Index Terms*—Fiber nonlinear optics, nonlinear Schrödinger equation, optical pulse compression, ultrafast optics.**

I. Introduction

ADVANCES in high peak power pulse delivery in optical fibers are opposed by the intensity dependent damage threshold. The demand for high peak power therefore necessitates an increase in core diameter which often results in multimode (MM) guidance. Although larger-mode area fibers extend the transmittable power, it remains ultimately limited by self-focusing. The critical self-focusing power is given as $P_{crit} = 1.86\lambda^2/(4\pi n_0 n_2)$ [1], where λ is the wavelength, n_0 the linear refractive index and n_2 the nonlinear index coefficient. For fused silica, P_{crit}~4.6 MW at $\lambda = 1.06\mu$m, which is comparable to the peak powers of ultrashort pulses that can be obtained using Yb doped fiber amplifiers [2]. Powers above P_{crit} are used in manufacturing, for example, to write permanent modifications to the refractive index of multimode fibers [3]. Quasi-stationary solutions to the spatio-temporal dynamics of fs pulses with powers of order of P_{crit} or beyond have also been investigated both experimentally and theoretically in the context of laser beam filamentation [4] and of light bullets propagating in nonlinear waveguide arrays [5].

For high-power pulse delivery through fibers however, significant self-focusing and subsequent fiber damage must be avoided. In the continuous-wave (CW) or long-pulse regime this is achieved with powers below P_{crit}. In this case the launched light can undergo periodic oscillations of the beam waist along the fiber as a result of the interplay between self-focusing, diffraction, and reflection at the fiber core-cladding interface, but the peak intensities remain below the damage level throughout propagation.

For *ultrashort, femtosecond pulses* the situation is more complicated, since then temporal effects can enhance the peak power beyond damage levels even for input peak powers well below P_{crit}. Studies in the anomalous dispersion regime of *bulk fused silica* describe extensively the compression of fs pulses in space and time (spatio-temporal focusing) [6]. Group-velocity dispersion, nonlinearity and self-steepening temporally compress the pulse. The resulting increase in peak power triggers transverse spatial compression and the spatially compressed regions may then be pushed to later times by group-velocity dispersion [7]. In normal dispersive bulk media, group-velocity dispersion can split the pulse temporally before spatial compression occurs [8]. Studies of self-focusing in bulk in general exceed the literature on self-focusing in fibers where one must also account for significant waveguide effects. Inside an optical fiber, the beam focuses, then diffracts, then gets reflected at the core cladding boundary before focusing again. Effectively, this instigates periodic transverse spatial oscillations which over larger distances may result in an evolution of the temporal profile distinguished from that of bulk. If the fiber guides multiple modes spatial self-focusing can be described through the periodic transfer of power between modes. To lowest order in perturbation theory, the maximum power in the first higher order mode is found to be proportional to the square of the wave-vector mismatch between the fundamental mode (FM) and the first higher order mode, while the period of the transfer is inversely proportional to the wave-vector mismatch [9]. The periodic exchange of power between modes eventually ceases as the modes go through a walk-off process caused by the intermodal group-velocity mismatch [9, 10].

The aim of this paper is to investigate the interaction of temporal and spatial pulse compression effects when high-peak power fs pulses propagate in MM optical fiber. We discuss the dominant mechanisms and identify pulse parameter regimes where fiber damage can be avoided. In Sec.

Manuscript received Month Day, 2012. The authors are with the Optoelectronics Research Centre, University of Southampton, Southampton SO17 1BJ, United Kingdom. G. Hesketh's email is gdh1e10@orc.soton.ac.uk

II we introduce our numerical model, discuss its validity, and give a numerical example of spatio-temporal pulse compression to highlight the main effects. In Sec. III we discuss the temporal effects alone, before detailing in Sec. IV how these are modified by spatial effects. We then discuss briefly the influence of Raman scattering and the dependence of our results on the pump wavelength in Sec. V. Finally we summarize and conclude our work in Sec. VI.

II. NUMERICAL MODEL

We herein utilize a description of ultrashort pulse propagation in MM fibers based on a MM generalized nonlinear Schrödinger equation (MM-GNLSE) [11] to demonstrate the spatio-temporal focusing of fs pulses launched with input peak powers $P_0 < P_{crit}$. The MM-GNLSE can be simulated numerically orders of magnitude faster than propagation based nonlinear envelope equation (NEE) methods [12,13] because of the relatively small number of modes involved; typically 6 to 10 modes ensure CW spatial resolution comparable with propagation based methods up to $\sim 0.9P_{crit}$ [14]. The model incorporates high-order dispersion, self-steepening, noise and Raman scattering. Plasma and multi-photon absorption effects are excluded and thus this work investigates the approach to damage without reference to damage itself. The evolution of the envelope of the p^{th} mode is described by:

$$\frac{\partial A_p}{\partial z} = i\sum_{n=0}\frac{\beta_n^{(p)}}{n!}\left(i\frac{\partial}{\partial t}\right)^n A_p(t) + \frac{in_2\omega_0}{c}\left(1+\frac{i}{\omega_0}\frac{\partial}{\partial t}\right)\mathcal{N}^{(p)}(t)$$

$$\mathcal{N}^{(p)}(t) = \sum_{l,m,n} Q_{plmn}A_l(t)\int \mathrm{d}\tau R(\tau)\,A_m(t-\tau)A_n^*(t-\tau)$$

$$Q_{plmn} = \frac{\int \mathrm{d}x\mathrm{d}y F_pF_lF_mF_n}{\left[\int \mathrm{d}x\mathrm{d}y F_p^2 \int \mathrm{d}x\mathrm{d}y F_l^2 \int \mathrm{d}x\mathrm{d}y F_m^2 \int \mathrm{d}x\mathrm{d}y F_n^2\right]^{1/2}}$$

$$R(t) = (1-f_R)\delta(t) + f_R h(t) \qquad (1)$$

Both material and waveguide dispersion are incorporated through the Taylor expansion of the modal propagation constant $\beta^{(p)}(\omega)$ about the central frequency ω_0 with coefficients $\beta_n^{(p)}$. The nonlinear coupling is governed by the overlaps Q_{plmn} of the transverse mode functions F_p which in this case are linearly polarized. Raman effects contribute with a fraction f_R and a temporal response function $h(t)$ to the fiber nonlinearity.

For the numerical simulations in this work we assume a step-index fiber with core radius $a = 31.25$ µm and core-cladding refractive index difference $\delta n = 0.015$ that supports 9 LP_{0n} modes in the near-infrared. Of these, we find the power coupled into modes n with $n \geq 4$ to be negligible in most of the presented cases. In the following we will focus on the case where the pump light is launched into the FM at its zero dispersion wavelength $\lambda_0^{(1)} = 1.269$ µm. At this wavelength $P_{crit} = 6.6$ MW. For pulses launched at shorter wavelengths, far in the normal dispersion regime, dispersion will quickly broaden the pulse temporally. In this case no spatio-temporal compression occurs and fiber damage is avoided, however after propagation the pulses will have to be re-compressed by external means in order to retain a high peak power pulse. By launching in the anomalous dispersion region, strong soliton compression occurs at the peak powers of interest here and pulse collapse occurs over very short distances. For high-power pulse delivery through fiber, launching at or near $\lambda_0^{(1)}$ is therefore of particular interest. We will return to the wavelength dependence of self-focusing in Sec. V.

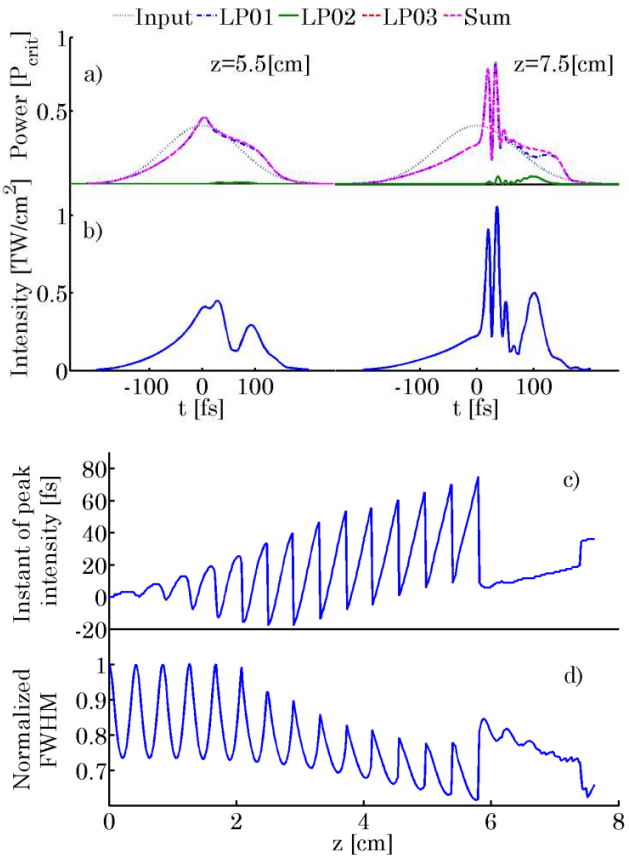

Fig. 1. Evolution of a 100 fs pulse launched with a peak power of $0.4P_{crit}$. The modal power distribution a) and the corresponding intensity (maximum over transverse spatial coordinates) distribution in time b) at two propagation distances. c) Instant of peak intensity of the pulse and d) the corresponding transverse spatial FWHM of the intensity profile.

As an example of spatio-temporal self-focusing Fig. 1a) shows the evolution of the modal power envelopes, $\left|A^{(p)}(z,t)\right|^2$, succeeding a Gaussian pulse launched into the FM with initial peak power $P_0 = 0.4P_{crit}$ and $1/e^2$ width $\tau_0 = 100$ fs. Dispersion and nonlinear effects compress the pulse in time and as a result the peak power tends to P_{crit} after about 7.5 cm of propagation. The corresponding intensity profile in Fig.1b) demonstrates that not all intensity peaks correspond to peaks in power: while the intensity maxima near $t = 0$ correspond to temporal compression of the pulse in the FM, the intensity peak at 100 fs results from the interference

of light fields in different modes, mainly of LP_{01} and LP_{02}. Fig.1c) shows that for $z \lesssim 6$ cm the peak intensity frequently sweeps across the trailing edge of the pulse due to the difference in modal propagation constants. The corresponding transverse spatial full width at half maximum (FWHM), Fig.1d), shows the expected periodic oscillations slowly damping out due to intermodal walk off [9,10]. For $z \gtrsim 6$ cm the temporal compression in the FM increases the peak power towards P_{crit} and the peak intensity of the leading edge rises above all the oscillations in the tail, Fig.1c). At the leading edge there is initially no power in the higher order modes but as the coupling restarts, the FWHM reduces, Fig.1d), and the intensity increases further to potentially damaging levels.

The maximum instantaneous pulse intensity corresponding to the simulation of Fig. 1 is shown in Fig. 2a). The initial periodic stage resembles continuous wave propagation and the beat period is $\sim 2\pi/\left(\beta_0^{(1)} - \beta_0^{(2)}\right)$ [9]. Comparing the MM simulation results with a simulation of the FM only, that is, with a simulation including only the temporal effects but neglecting spatial self-focusing, shows that peak intensities are significantly higher in the full model. However, the single-mode (SM) model predicts correctly the onset of enhanced self-focusing due to temporal effects, thus giving a qualitative description of the complex spatio-temporal dynamics.

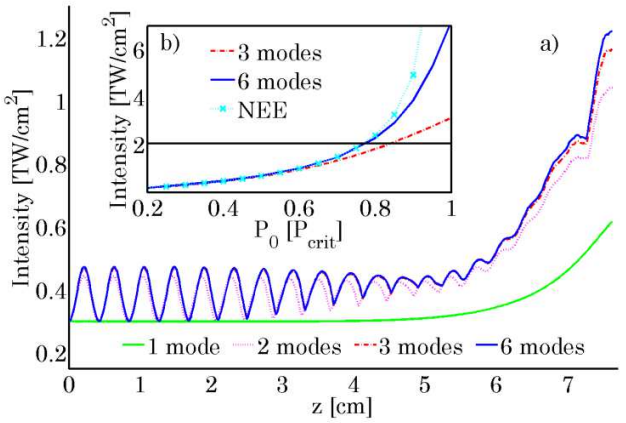

Fig. 2. a) Peak intensity evolution (maximum over time and transverse spatial coordinates) with propagation distance for the launch conditions in Fig. 1, approximated by 1, 2, 3 and 6 modes. b) Maximum intensity under CW pumping in the FM, approximated by 3 and 6 mode MM-GNLSE simulations and by solutions of the NEE.

Fig. 2a) also investigates the convergence of the MM-GNLSE approach showing simulations with 2, 3 and 6 modes. Simulations with only two modes already show some differences with intensities below ~0.5 TW/cm^2, but the 3 and 6 mode approximations are indistinguishable at intensities below 0.8 TW/cm^2 and differ by at most $\sim 5\%$ between $0.8 - 1.2$ TW/cm^2. Fig. 2b) shows the maximum intensity reached by 3 and 6 mode simulations for CW pumping in the FM as a function of input peak power. Resolution is lost with 3 modes at intensities above ~2 TW/cm^2 (black-solid line) which corresponds to input powers of $P_0 \cong 0.8 P_{crit}$. Comparison with simulations of the NEE [12,13] in the CW regime, indicated by crosses in Fig. 2b), show that 6 mode simulations are accurate to within $\sim 7\%$ at intensities of ~4 TW/cm^2 for the chosen fiber.

Ionization in silica occurs from a threshold electric field of 30 MV/cm [15] corresponding to 4.7 TW/cm^2 and bulk optical breakdown has been reported at around 10 TW/cm^2 [16]. We therefore conclude that the MM-GNLSE approach is reliable up to the material damage threshold. For intensities higher than this an accurate model would have to include more modes to achieve the required spatial resolution as well as optical nonlinearities related to ionization and plasma effects.

III. TEMPORAL FOCUSING: THE SM CASE

The numerical example of Figs. 1 and 2 showed that the temporal compression of laser pulses in the fundamental mode may be responsible for defining the onset of enhanced self-focusing. As a first step in our discussion of the parameter dependence of these effects we will therefore investigate in detail the temporal effects alone before comparing the results with full simulations in Sec. IV. To this end we confine the simulations to the FM alone, thereby eliminating the transverse spatial degrees of freedom. As a simple reference model we also neglect Raman scattering in this section.

The dominant mechanism responsible for temporal compression in the FM with pumping at the zero-dispersion wavelength $\lambda_0^{(1)}$ is the interaction of self-phase modulation with third order dispersion (TOD). For pulse lengths $\tau_0 > 10$ fs we find 4th order dispersive effects at $\lambda_0^{(1)}$ to be much smaller than 3rd order effects and thus a SM simulation is well approximated by TOD exclusively. TOD is parameterized by the third order coefficient $\beta_3^{(1)}$ and has the associated TOD length $L_3^{(1)} = {\tau_0}^3/\beta_3^{(1)}$. Nonlinear effects are characterized by the nonlinear length ${L_{NL}}^{(1)} = 1/\left(\gamma^{(1)} P_0\right)$ of the FM where the nonlinear parameter is defined as $\gamma^{(1)} = n_2 Q_{1111}\omega_0/c$. For our specific fiber $\beta_3^{(1)} = 1.23 \times 10^{-5}\,\mathrm{ps^3/m}$ and $\gamma^{(1)} = 0.08\,\mathrm{W^{-1}km^{-1}}$. Using these definitions, pulse propagation can be described by the dimensionless single mode equation:

$$\frac{\partial}{\partial Z} U = r \frac{\partial^3}{\partial T^3} U + \left(i - s\frac{\partial}{\partial T}\right)|U|^2 U \qquad (2)$$

where $r = \mathrm{sign}\left[\beta_3^{(1)}\right] {L_{NL}}^{(1)}/\left(6 {L_3}^{(1)}\right)$, $s = 1/(\omega_0 \tau_0)$, $T = t/\tau_0$, $Z = z/{L_{NL}}^{(1)}$ and $U = A^{(1)} P_0^{-1/2}$ are the ratio of the nonlinear and third order dispersion lengths, the self-steepening parameter and the normalized time, propagation distance and envelope, respectively. Self-steepening effects cannot be ignored. Self-steepening always steepens the trailing edge, whereas TOD tries to steepen the leading/trailing edge when $\mathrm{sign}\left[\beta_3^{(1)}\right] = +/-$. As energy is conserved in Eq. (2) the net result is that when the two effects are comparable, self-steepening counterbalances TOD and suppresses peak power increase when $\beta_3^{(1)} > 0$ and enhances it otherwise. We

hereafter focus on $\beta_3^{(1)} > 0$, as is typical in large fibers where material dispersion dominates over waveguide dispersion, such that self-steepening opposes peak enhancement.

For various r, s values, chosen to encompass the fs and MW pulse regime of our fiber, Fig. 3 shows the (dimensionless) maximum peak, $M(r,s)$, recorded during propagation for a Gaussian pulse launched with unity peak and width. The fiber length is restricted to $L = 14{L_{NL}}^{(1)}$ $(Z = 14)$ here as modulation instability starts to create high-intensity noise peaks from $L \approx 16{L_{NL}}^{(1)}$ [17]. We identify the region (green-solid line Fig. 3):

$$34.27s - 5.75 < \log_{10} r < -5.49s^2 - 2.91s - 2.1 \quad (3)$$

with $0 < s < 0.087$, as bounding the area of parameter space within which temporal compression increases the peak above 1%. The region of large peak enhancement in the large s, small r, corner is the result of self-steepening alone and corresponds to launching very short, very high peak power pulses [18], which do not form the focus of this work. If $\log_{10} r > -5.49s^2 - 2.91s - 2.1$ then TOD is strong and the pulse broadens without peak enhancement. If $\log_{10} r < 34.27s - 5.75$ then TOD is weak and no pulse reshaping occurs at all. In addition to (3), we give the r value at which the largest temporal compression is recorded, r_{crit} (blue-dashed line Fig. 3), and the corresponding recorded peak value, $M(r_{crit}, s)$:

$$\log_{10} r_{crit}(s) \cong -260.7s^2 + 45.75s - 4.97 \quad (4)$$

$$M(r_{crit}, s) \cong 0.063/(s + 0.014) + 4.32s \quad (5)$$

where again $0 < s < 0.087$. The length at which M is recorded Z_M is plotted in Fig. 3b). In the region of significant compression it does not vary much with s and is roughly approximated by $Z_M \cong -4.77 \log_{10} r - 8.26$.

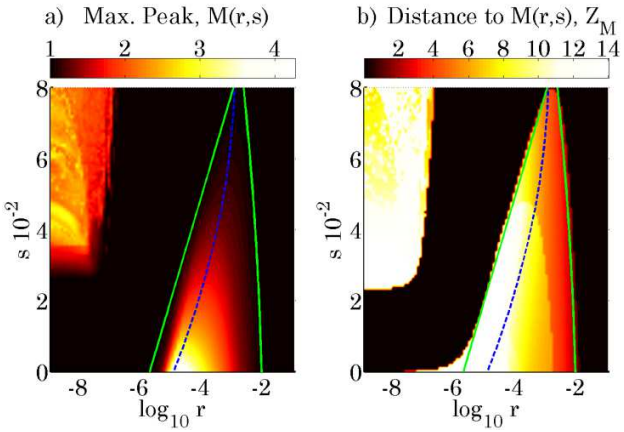

Fig. 3. a) $M(r,s)$ for SM propagation, (1), green-solid line isolates the region where temporal compression enhances the peak more than 1%, blue-dashed line indicates the largest peak enhancement by temporal compression for given s. b) Z_M, the length at which M was recorded.

Equations (3)-(5) together with Fig. 3 predict how the beam would hypothetically evolve without the influence of the higher-order modes. In the following we will discuss the modification of the pulse dynamics due to spatial effects.

IV. SPATIO-TEMPORAL FOCUSING: THE MM CASE

Including the higher order modes, i.e. transverse spatial effects, complicates the picture with a multitude of dispersion and nonlinear modal parameters such that dimensionless characterization like that in Fig. 3 is impractical. The leading contributions to the intermodal dispersion stem from the mismatched propagation constants, $\beta_0^{(1)} - \beta_0^{(2)}$, and group-velocity related terms, $\beta_1^{(1)} - \beta_1^{(2)}$, in the fundamental and first higher order modes, while higher order dispersion in the higher order modes plays a relatively minor role in the dynamics of the total pulse envelope. For the simulations presented in this section, the power in the higher order modes $n > 3$ remains relatively small for a fundamental mode launch except when peak intensities exceed ~2 TW/cm^2, see Fig. 2.

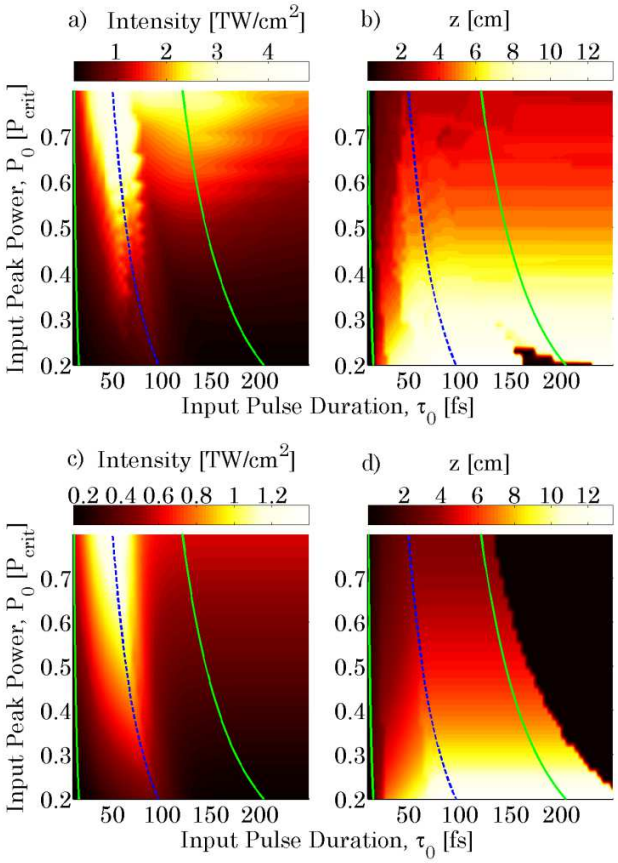

Fig. 4. a) Maximum intensity recorded over $L = 14{L_{NL}}^{(1)}$ as a function of launch conditions, simulated by the 3-mode MM-GNLSE, and b) the length at which the maximum intensity was recorded (physical units). c),d) the corresponding SM case (Note: different color scales). The analytic expressions for position of largest peak intensity (Eq. (4), blue dashed) and region of significant compression (Eq. (3), green solid) are also shown.

Fig. 4 compares pulse compression calculated using the

MM-GNLSE, Eq. (1), that incorporates Raman scattering, self-steepening and modal dependent dispersion profiles, with the SM approximation, Eq. (2). Spatio-temporal effects lead to compression and potentially to damaging intensity levels for launched pulse durations in a narrow region around 50 fs with launched peak powers $> 0.5P_{crit}$. Interestingly, although the maximum intensities reached in the full spatio-temporal dynamics are much higher than for the temporal (SM) calculations, the pulse parameter regimes that look unsafe for pulse delivery through fiber are very well described by the simplified SM case. To show this clearly, the blue-dashed line in Fig. 4 represents the largest peak intensity fit in the SM case, Eq. (4), in physical units. Furthermore, the propagation length at which significant compression occurs is also similar for the MM and the SM case, in agreement with the numerical example of Fig. 2. Note that the CPU time of this large scale parameter scan meant it was necessary to limit the simulation to 3 modes here instead of 6. As mentioned previously, where the intensity rises above ~ 2 TW/cm^2 in Fig. 4, the 3 mode approximation begins to lose resolution and it is expected that in reality the intensity would be even higher, thus approaching or exceeding damage levels [15,16]. Nonetheless, comparisons with MM-GNLSE simulations with larger mode numbers indicate the 3 mode results are accurate if the maximum intensities remain below this value and Fig. 4 therefore gives a reliable depiction of parameter regimes where fiber pulse delivery is possible without damage.

As a specific example of spatio-temporal focusing, Figs. 4 a), b), we give explicit simulation results for a pulse launched with an input width $\tau_0 = 60$ fs and input peak power $P_0 = 0.5P_{crit}$, corresponding to an input intensity of ~ 0.4 TW/cm^2. Spatio-temporal compression occurs over a distance $z = 5$ cm and generates an intensity of ~ 2 TW/cm^2. In comparison, Fig. 4 c) indicates launching the same pulse in the SM approximation, i.e. without spatial focusing, would generate an intensity of ~ 0.9 TW/cm^2 while Fig. 2 b) indicates that for such input power spatial focusing alone would produce an intensity of ~ 0.7 TW/cm^2 in a CW launch. It is thus inferred that for the pulse parameters in the example, spatial and temporal focusing effects are comparable and that their combination results in the observed intensity.

Figure 4 shows the maximum intensity, relevant for fiber damage by ionization, yet for a further understanding of the pulse dynamics it is also instructive to look at the maximum pulse power (summed over modes) reached during propagation. To this end, we show in Fig. 5 the ratio of the maximum power in the MM case over that in the SM case. For relatively long pulses, to the right of the area given by Eq. 3 (green solid line), little temporal compression occurs in both SM and MM simulations. Thus, while spatial effects may increase the local intensity, the local power integrated over the transverse beam profile remains constant. In this regime the pulse dynamics mimics the CW picture and the maximum intensity as a function of input power follows the one previously shown in Fig. 2b). However, at shorter pulse durations, the higher order modes also alter the temporal dynamic relative to the SM approximation resulting in a redistribution of power along the pulse and thus in a change of peak power values. Fig. 5 shows that these effects lead to a reduction of maximum peak power to the left of the line given by Eq. (4) and to an enhancement of peak power to the right of it. Thus the point of maximum peak power is shifted towards longer pulse lengths compared to the SM simulation. This is in contrast to Fig. 4 where the peak *intensities* are reached for the same parameters. This indicates that maximum peak powers and peak intensities are not necessarily co-located due to the interaction of multimode nonlinear and dispersive effects. The MM simulations seem to indicate a general reduction in peak powers at very high launch powers, but given that the simulations lose accuracy there this result is inconclusive.

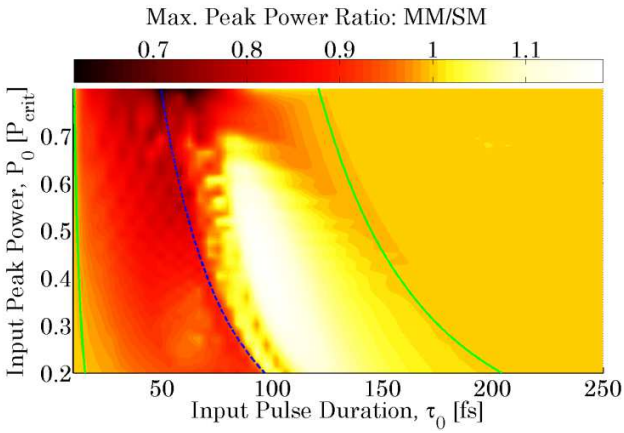

Fig. 5. Maximum peak power: ratio of MM case to SM case. In dark regions spatial focusing reduces temporal compression, in bright regions spatial focusing enhances temporal compression. Blue-dashed line shows maximum compression, Eq. (4), green-solid lines indicate area of significant compression, Eq. (3), in SM simulations.

V. RAMAN SCATTERING EFFECTS AND PUMP WAVELENGTH DEPENDENCE

The MM-GNLSE results presented in the previous section included Raman scattering. To identify its role in spatio-temporal pulse compression, we performed another set of simulations excluding the Raman effect, see Fig. 6. The results show that Raman scattering can reduce or enhance peak intensities depending on pulse parameters by up to ~50%.

For relatively long pulses, $\tau_0 > 100 - 150$ fs, where temporal reshaping is weak, Raman scattering can significantly enhance peak intensities. Here, the higher order modes are receiving gain at the expense of the FM, which enhances the spatial compression, a process known as Raman enhanced self-focusing [19, 20]. Conversely, for short pulses, $\tau_0 \lesssim 100$ fs, where the pulse duration becomes comparable to the Raman response time of 32 fs [21], Raman scattering starts to reduce temporal coherence and counteracts temporal compression, leading to a reduction in peak intensity. Thus, in

both regimes Raman scattering has the potential to significantly modify the spatio-temporal dynamics.

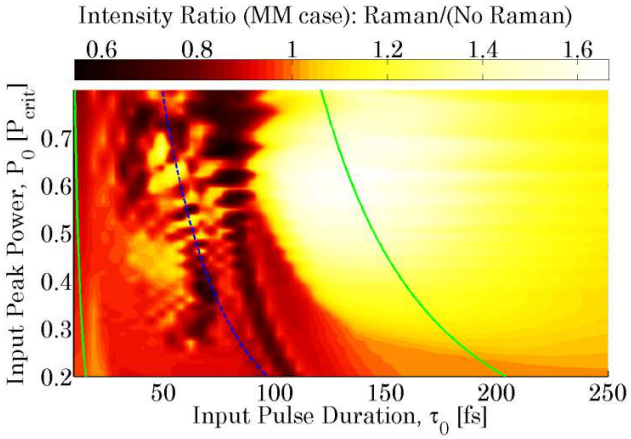

Fig. 6. Maximum intensity reached in MM simulations: Ratio of simulation including Raman scattering to simulation excluding it. Blue-dashed line by Eq. (4), green-solid lines by Eq. (3).

Finally, we briefly discuss the dependence of spatio-temporal self-focusing on the pump wavelength. For only a small shift of the pump from the zero-dispersion wavelength, e.g. to $\lambda_0^{(1)} + 5$ nm, Fig. 7a), the behaviour is not altered significantly. For a launching wavelength of $\lambda_0^{(1)} + 100$ nm, Fig. 7b), a shift slightly larger than the spectral bandwidth of the input pulse, similar effects are visible, yet second order dispersion is dominant and drives large peak power increase at shorter fiber lengths. For even longer pump wavelengths, massive compression at short propagation distances is observed. For a launching wavelength of $\lambda_0^{(1)} - 100$ nm, a shift into the normal regime comparable to the bandwidth of the input pulse, Fig. 7c), no compression occurs and the pulse broadens in time. As already mentioned in Sec. II, for pump wavelengths far in the normal dispersion regime dispersion effects dominate and the pulse quickly broadens.

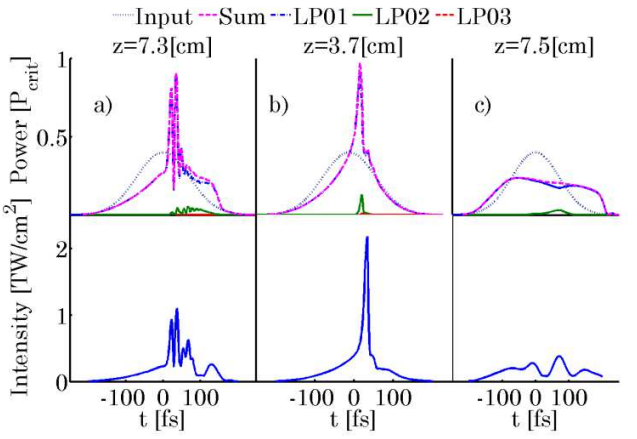

Fig. 7. Pulse propagation with the same parameters as Fig.1 launched at three central wavelengths, a) $\lambda_0^{(1)} + 5$ nm: similar to Fig.1, b) $\lambda_0^{(1)} + 100$ nm: strong temporal compression at short length, c) $\lambda_0^{(1)} - 100$ nm: strong temporal broadening. Power shown on top, corresponding intensity below (maximum over transverse spatial coordinates).

VI. CONCLUSION

In summary, we analyzed the impact of spatio-temporal compression on short-pulse transmission through multimode fibers for launched peak powers approaching the critical power for pulse collapse by self-focusing. We find that the onset of enhanced spatial compression by temporal effects which leads to potential fiber damage is mainly determined by temporal compression in the fundamental fiber mode. A simplified single-mode model therefore serves as a good indicator to identify critical pulse parameters. As a consequence, for pump pulses launched at or near the zero-dispersion wavelength of the fundamental mode we find that the interaction of third order dispersion and nonlinear effects largely governs maximum pulse powers and propagation lengths if one is to avoid damage. We emphasize, however, that the exact dynamics, and the actual intensity levels reached, can only be obtained by solving the complex multi-dimensional propagation equations or, as done in this paper, the multimode generalized nonlinear Schrödinger equation in order to include all intermodal dispersion and nonlinear effects. It was also shown that the inclusion of Raman scattering is essential for accurate modeling. We finally verified that our main conclusions still hold for pump wavelengths shifted away from the zero-dispersion wavelength as long as the shift is comparable to the pulse spectral width.

For the specific fiber parameters used in this paper (31.25 µm core radius), damage intensity levels are reached for pulses with durations in a relatively narrow region around 50 fs and with powers exceeding 50% of the critical power for (CW) self-focusing. Typical propagation distances before damage occurs are of the order of a few cm. For large mode area fibers, dispersion is mainly determined by material dispersion, thus scaling the fiber size will mainly affect the nonlinear effects discussed here via a reduction of the nonlinear effects inversely proportional to the square of the fiber diameter. Thus, scaling the fiber core up to about 100 µm radius will allow for fiber-based transmission of fs pulses with powers close to the critical power over approximately 50 cm.

REFERENCES

[1] G. Fibbich and A.L. Gaeta, "Critical power for self-focusing in bulk media and in hollow waveguides," *Opt. Lett.*, vol. 25, pp. 335-37, 2000.

[2] A. Galvanauskas, M.Y. Cheng, K.C. Hou, and K.H. Liao, "High peak power pulse amplification in large-core Yb-doped fiber amplifiers," *IEEE J. Sel. Top. Quantum Electron.*, vol. 13, pp. 559-66, 2007.

[3] S.H. Cho, H. Kumagai, and K. Midorikawa, "Fabrication of multi-core structures in an optical fiber using plasma self-channeling," *Opt. Express*, vol. 11, no. 15, pp. 1780-1786, 2003.

[4] A. Couairon and A. Mysyrowicz, "Femtosecond filamentation in transparent media," *Phys. Rep.*, vol. 441, pp. 47-189, 2007.

[5] F. Eilenberger et al., "Evolution dynamics of discrete-continuous light bullets," *Phys. Rev. A, vol. 84*, 013836, 2011.

[6] S.L. Chin et al., "The propagation of powerful femtosecond laser pulses in optical media: physics, applications, and new challenges," Can. J. Phys., vol. 83, no. 9, pp. 863-905, 2005.

[7] L. Berge and S. Skupin, "Self-channeling of ultrashort laser pulses in materials with anomalous dispersion," *Phys. Rev.E* , vol. 71, 65601, 2005.
[8] J.E. Rothenberg, "Pulse splitting during self-focusing in normally dispersive media," *Opt. Lett*., vol. 17, no. 8, pp. 583-85, 1992.
[9] G. Tempea and T. Brabec, "Theory of self-focusing in a hollow waveguide," *Opt. Lett.*, vol. 23, no. 10, pp.762-764, 1998.
[10] F. Poletti and P. Horak, "Dynamics of femtosecond supercontinuum generation in multimode fibers," *Opt. Express*, vol. 17, pp. 6134-6147, 2009.
[11] F. Poletti and P. Horak, "Description of ultrashort pulse propagation in multimode optical fibers," *J. Opt. Soc. Am. B*, vol. 25, pp.1645-54, 2008.
[12] T. Brabec and F. Krausz, "Nonlinear optical pulse propagation in the single-cycle regime," *Phys. Rev. Lett.*, vol. 78, no. 17, pp. 3282-3285, 1997.
[13] J.K. Ranka and A.L. Gaeta, "Breakdown of the slowly varying envelope approximation in the self-focusing of ultrashort pulses," *Opt. Lett.*, vol. 23, no. 7, pp. 534-536, 2009.
[14] P. Horak and F. Poletti, "Multimode nonlinear fibre optics: theory and applications" in *Recent Progress in Optical Fiber Research*, edited by M. Yasin, S.W. Harun, and H. Arof, pp. 3-25, Rijeka: InTech, 2012.
[15] D. Du, X. Liu, G. Korn, J. Squier, and G. Mourou, "Laser-induced breakdown by impact ionization in SiO2 with pulse widths from 7 ns to 150 fs," *App. Phys. Lett.*, vol. 64, no. 23, pp. 3071-3073, 1994.
[16] C.B. Schaffer, A. Brodeur, and E. Mazur, "Laser-induced breakdown and damage in bulk transparent materials induced by tightly focused femtosecond laser pulses," *Meas. Sci. Technol.*, vol. 12, pp. 1784-1794, 2001.
[17] J.M. Dudley, G. Genty, and S. Coen, "Supercontinuum generation in photonic crystal fiber," *Rev. Mod. Phys*, vol. 78, pp. 1135-84, 2006.
[18] A. Gaeta, "Catastrophic collapse of ultrashort pulses," *Phys. Rev. Lett.*, vol. 84, pp. 3582-3585, 2000.
[19] G. He, D. Liu, and. S. Liu, "Coherent Raman spectra and Raman-enhanced self-focusing in multimode fiber," *Opt. Commun.*, vol. 70, no. 2, pp. 145-50, 1988.
[20] K.S. Chiang, "Stimulated Raman scattering in a multimode optical fiber: self-focusing or mode competition?" *Opt. Commun.*, vol. 95, no. 4, pp. 235-38, 1992.
[21] G.P. Agrawal, *Nonlinear Fiber Optics*, 4th ed., San Diego, CA: Academic, 2007.